In situ study of the annealing behavior of porosity in icosahedral Al-Pd-Mn quasicrystals using third generation x-ray synchrotron radiation imaging

S. Agliozzo
European Synchrotron Radiation Facility, Boîte Postale 220, F-38043 Grenoble cedex, France
and Institute for Scientific Interchange Foundation, Villa Gualino, Viale Settiminio 65, I-10133 Torino, Italy

J. Gastaldi
CRMC2-CNRS, Campus de Luminy, case 913, F-13288 Marseille cedex 09, France

H. Klein
Laboratoire de Cristallographie, 25 avenue des Martyrs, Boîte Postale 166, F-38042 Grenoble cedex 9, France

J. Härtwig and J. Baruchel
European Synchrotron Radiation Facility, Boîte Postale 220, F-38043 Grenoble cedex, France

E. Brunello
Dipartimento di Scienze Fisiologiche, Università degli Studi di Firenze, Viale G.B. Morgagni 63, I-50134 Firenze, Italy
(Received 22 May 2003; revised manuscript received 1 December 2003; published 6 April 2004)

The evolution of porosity in an icosahedral Al-Pd-Mn quasicrystal single grain has been studied *in situ* during an annealing at 800 °C. A drastic shrinkage of pores was observed and interpreted in the frame of a vacancy-mediated diffusion model.

DOI: 10.1103/PhysRevB.69.144204 PACS number(s): 61.72.Qq

I. INTRODUCTION

Quasicrystals are solids that exhibit long-range atomic order but no periodicity. A striking property of quasicrystals is the possibility to observe ''noncrystallographic'' rotational symmetries, e.g., fivefold symmetry axes. Despite the great theoretical and experimental efforts since the discovery of quasicrystals in the mid 1980's,[1] the determination of the structure of real quasicrystals has not been completed yet.[2,3]

The highly complex structures of quasicrystals result in peculiar physical properties that differ from those of metals, even though quasicrystals are in general constituted in majority of atoms that form metals in their elementary state. In order to elucidate further the dependence of the physical properties on the structure, it is necessary to obtain quasicrystals with a structure as perfect as possible, since defects are believed to have a great impact on the physical properties. In recent years quasicrystals were grown with a high quality showing rocking curve widths comparable to those of the best metallic crystals.[4] Nevertheless porosity is systematically observed in the submicrostructural[5] and microstructural[6] levels in the volume of Al-Pd-Mn quasicrystals.

Unlike pores observed in crystals (e.g., pure Al, Al alloys), pores in icosahedral Al-Pd-Mn quasicrystals occupy a rather high volume fraction, and their size can also be approximately 1000 times bigger in the quasicrystal than in the simple metal.[7] The formation mechanisms of pores known from crystals do not seem to explain satisfactorily porosity in quasicrystals and hence the origin of these pores remains still unclear.

Two hypotheses have been proposed to explain the occurrence of porosity. The first hypothesis suggests that pores are generated from the condensation and migration of thermal vacancies.[8] In the second one pores are interpreted as an intrinsic characteristic of the quasicrystalline structure.[9] These two hypotheses correspond to different approaches, but at the current stage, there is no experimental evidence that proves unquestionably the overall validity of one or the other.

The previous annealing experiments have shown changes in the shape and size of the pores.[6,8,10] The mechanism of these changes, however, is not elucidated even though it could give valuable information of the formation of porosity in quasicrystals. The aim of this work is to present the porosity evolution during a high-temperature annealing carried out on an icosahedral Al-Pd-Mn quasicrystalline single grain and studied *in situ* using synchrotron x-ray phase contrast radiography.

II. EXPERIMENTAL PROCEDURE AND SAMPLES

The experiments were carried out at the ID19 beam line of the European Synchrotron Radiation Facility (ESRF) in Grenoble, France. This beam line, dedicated to x-ray imaging and high-resolution diffraction, is characterized by a very long source-to-sample distance (145 m) and a small angular source size seen from a point of the sample (0.1–1 μrad). The beam was monochromated by two perfect Si crystals diffracting in the vertical plane in the $(+,-)$ nondispersive setting. The spectral width was $\Delta\lambda/\lambda \approx 10^{-4}$. The small source size (≈ 100 μm) combined to the long source-to-sample distance provides a large transverse coherence length (≈ 40 μm for the used wavelength of 0.516 Å), a feature fundamental to phase contrast imaging.[11,12]

The experimental layout is given in Fig. 1. Different im-

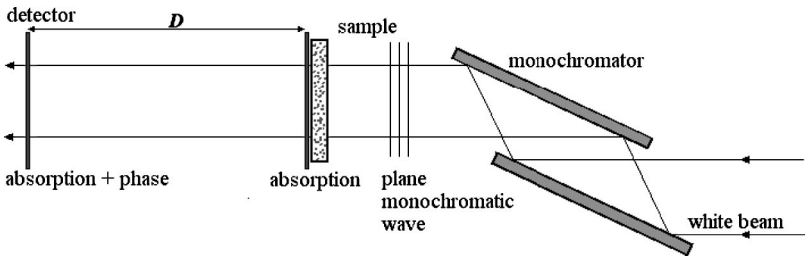

FIG. 1. Experimental layout for phase contrast radiography. Changing the sample-to-detector distance *D*, different imaging regimes can be probed.

aging regimes can be accessed by simply changing the sample-to-detector distance.[11] Experimental pore images were recorded at a fixed distance of 30 cm, which gives a good compromise for contrast from small and big pores, given a wavelength λ equal to 0.516 Å. This wavelength (just before a palladium absorption edge) was chosen to get a good transmission of the x-ray beam and to obtain a good contrast for small and big pores. The phase contrast radiographs were recorded by a (charge-coupled device) CCD-based online detector that consists of a scintillator to convert x-rays into visible light, coupled to a CCD camera with a microscope objective. The camera is a 14-bits CCD with a 1024×1024 (or 2048×2048) pixel array, developed at the ESRF and called FRELON (Fast REadout LOw Noise).[13] The optics associated to the detector provides a spatial resolution of the order of $1-2$ μm. Pore images sizes were measured precisely by a computer-aided detection of pore images from radiographs. Due to the experimental imaging process the pore image sizes are not identical to the sizes of the pores themselves. The true pore sizes have therefore been obtained using a calibration curve, which reports the correspondence between the measured pore sizes and the real ones. This curve was obtained by measuring, with the same detection software, the size of simulated pore images calculated in the same experimental conditions. The correspondence between experimental and simulated pore images was very good.[7] Note that the size of a pore is defined as the diameter of the sphere, which circumscribes its dodecahedral shape. The studied sample was grown by Czochralski method with a withdraw rate of 5.4 mm/h and in an argon atmosphere. No homogenization treatment was carried out after the growth. It was a plate shaped single crystal with a composition of $Al_{68.8}Pd_{24.0}Mn_{7.2}$ and a thickness of about 380 μm.

The high-temperature treatment was carried out in an unstrained sample heated in an ultrahigh-vacuum chamber designed at the CRMC2 (Marseille, France). It is equipped with (a) two mirrorlike aluminum windows, obtained by the same techniques used to polish silicon wafer[14] (finishing treatment with an alumina solution down to 0.2 μm), which prevent spurious contrast in radiographs, (b) a pumping unit composed of a dry primary pump, a turbo pump, two ionic pumps, and a titanium sublimator, ensuring a vacuum of $10^{-8}-10^{-9}$ mbar at 800 °C, (c) a high-temperature furnace (maximum temperature 1000 °C) where the sample is mounted in a medium frame and heated by radiation coils in order to minimize the effect of thermal stress. The temperature was controlled by a thermocouple sensor placed close to the heating coil. The sample temperature was calculated using a calibration curve obtained prior to the experiment by heating the furnace with a second thermocouple sensor located at the sample position.

The sample was annealed at 800 ° C in two annealing cycles whose thermal profile is shown in Fig. 2. A first short annealing cycle of ~5 h was carried out in order to study whether changes at high temperature in the radiographic contrast recover to the initial state once the temperature is rapidly lowered back to room temperature. A second ~27 h long cycle was performed to observe the evolution of changes during a long stay at high temperature. The sample was heated and cooled with a rate of 20 °C/min. Note that the first annealing cycle is characterized by two stays at 600 °C and 770 °C. These stays allowed us to recover good vacuum conditions inside the high-vacuum chamber, but they were not necessary for further annealing cycles.

The sample was mechanically polished on both surfaces before experiments. This polishing was performed with diamond paste down to 1 μm in order to have high quality surfaces which do not introduce artifacts in phase contrast radiographs. The chemical composition of every sample was measured by energy dispersive spectroscopy (EDS) in a scanning electron microscopy (SEM) and no second phases were detected.

III. RESULTS

Figure 3 reports two phase contrast radiographs of a large region of the sample recorded before and after the two annealing cycles. In its as-grown state, the sample has in the

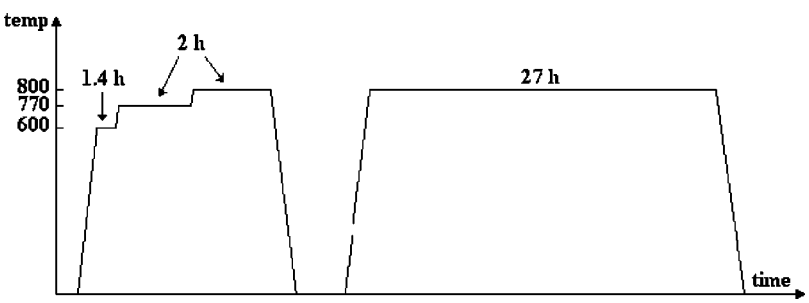

FIG. 2. Annealing layout composed of two cycles. A shorter one of ~5 h and a long one of ~27 h.

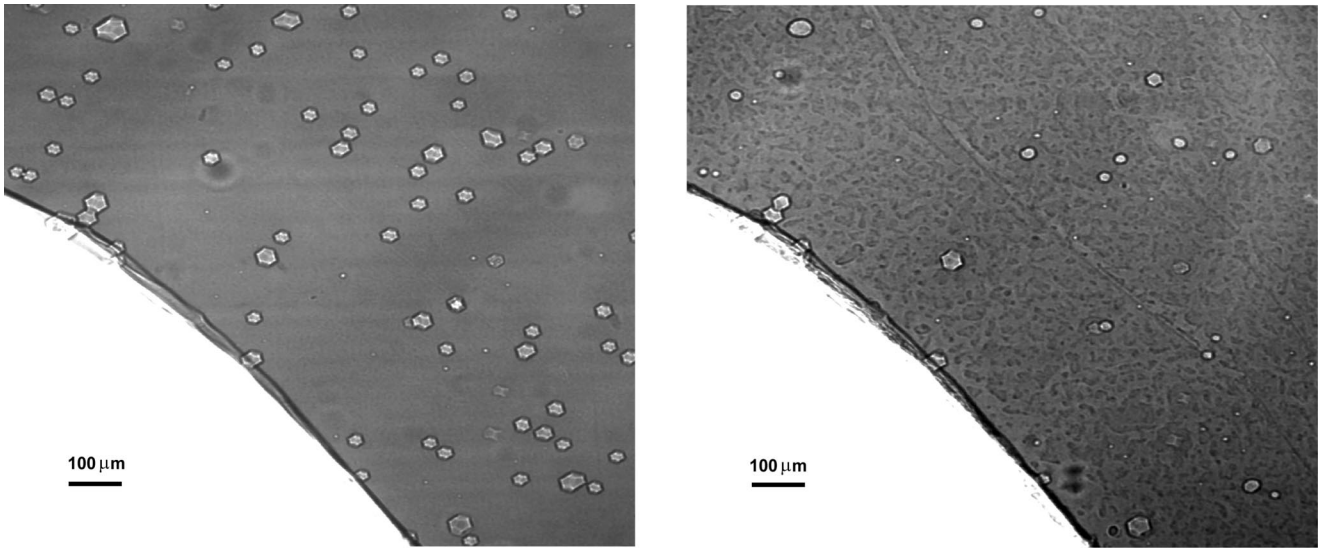

FIG. 3. Phase contrast radiographs (a) before and (b) after the long annealing.

bulk micrometric pores of dodecahedral shape. These pores are viewed along a twofold axis of the dodecahedron. The projection onto the image plane results in its hexagonal shape. The bright contrast lines inside the pore image stem from the projection of the edges of the dodecahedron [Fig. 3(a)]. After the annealing, the size of most pores decreases. Only the size of a few pores did not change. Moreover the state of the surface changes drastically from smooth to rough, resulting in an orange skinlike contrast in the images.

Pores whose size did not change after the annealing were located on the surface of the sample surface as shown by SEM micrographs in Fig. 4. This figure is composed of a phase contrast radiograph [Fig. 4(a)] and two SEM micrographs of both surfaces of the sample [Figs. 4(b) and 4(c)]. The pores that did not shrink during the annealing, correspond to the surface pores visible in SEM (marked by a circle in both images).

Figure 5 shows the porosity evolution in a small region of the sample during both annealing cycles. The size of pores decreases very rapidly during the first annealing cycle [Figs. 5(b) and 5(c)]. Moreover the shape of pore images changes from faceted [Fig. 5(c)] to round and the white line contrasts inside the pore images due to the edges of the dodecahedral shape of the pores disappear. During the second annealing cycle [from Figs. 5(e) to 5(k)], the sizes of the pores decrease further, even though less rapidly than in the first annealing cycle. The shapes of the pore images become more and more round with the annealing time. After cooling the sample at the end of the second annealing cycle, the pore images in the radiograph recorded at room temperature [Fig. 5(l)] do not show any visible change in the size and shape with respect to the pore images in the radiograph before the cooling of the sample [Fig. 5(k)].

Figure 6 shows scanning electron micrographs of two typical pores recorded before and after the annealing. Before annealing, the pore has a dodecahedral shape with sharp edges. After annealing, additional facets have appeared on the edges and corner as observed by Beeli *et al.*[8] These ad-

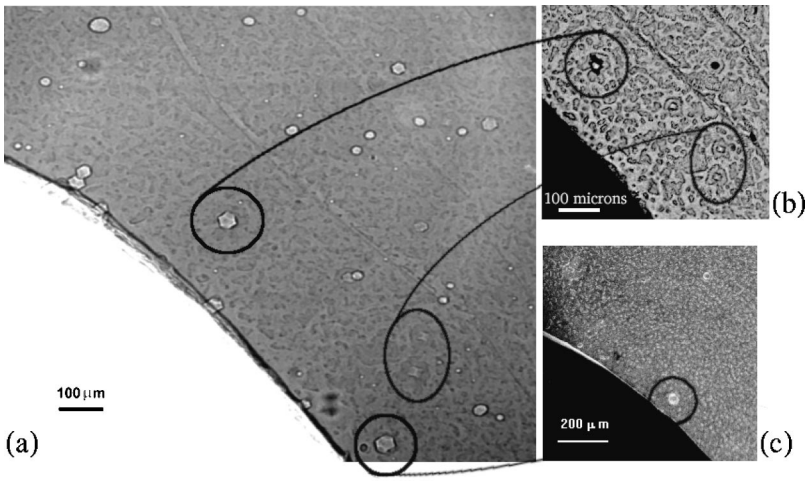

FIG. 4. Comparison between (a) a phase contrast radiograph and (b), (c) SEM micrographs of both sample surfaces, for the same region of the sample. Note the correspondence among pores surrounded by circles on both types of images.

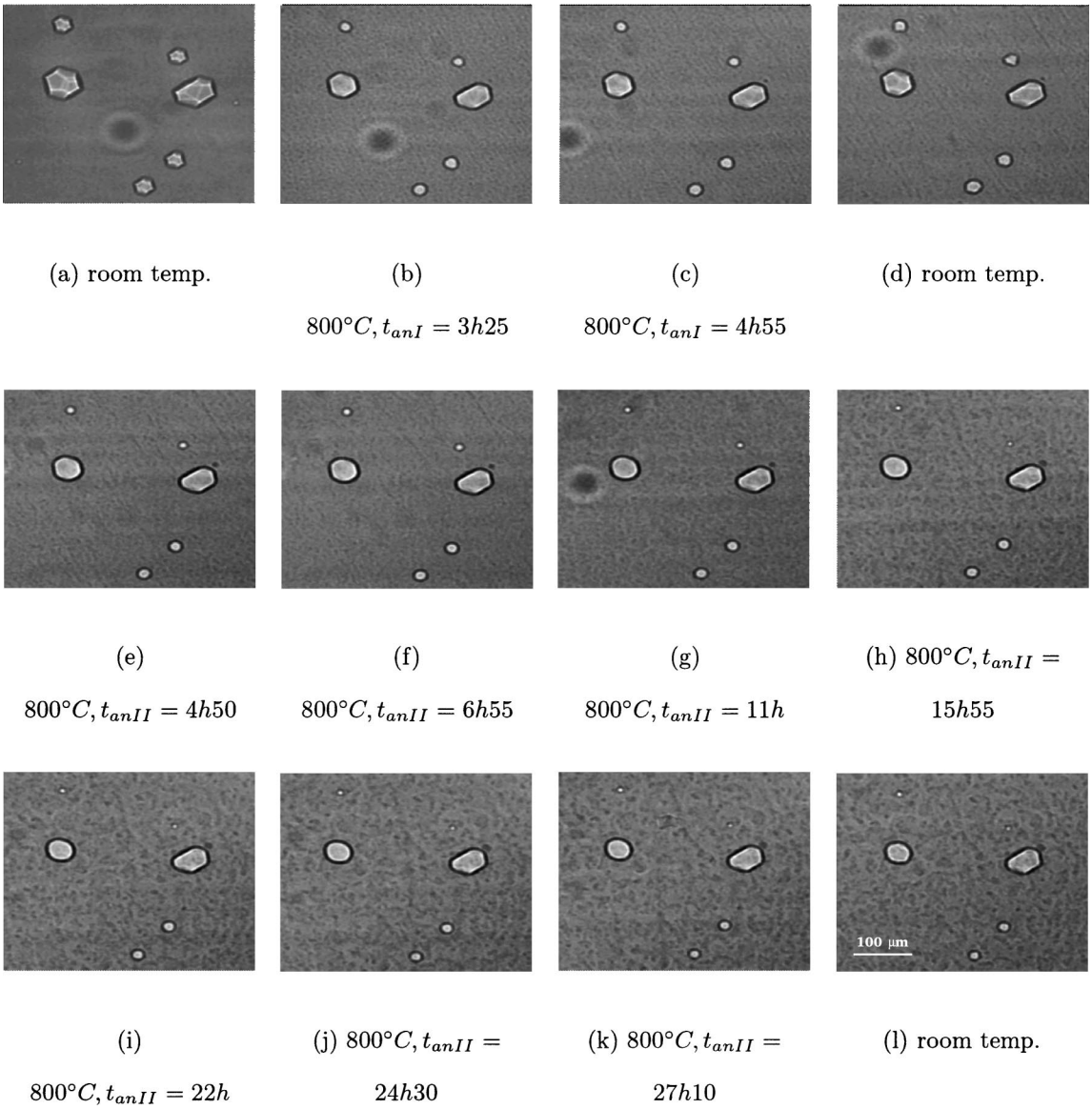

FIG. 5. Phase contrast radiographs of a small region of the sample recorded during both annealing cycles. The radiographs of the first annealing cycle are reported from (a) to (d), whereas those of the second annealing cycle start from (e). $\lambda = 0.516$ Å, sample to detector distance $D = 30$ cm. FRELON camera.

ditional facets result in the disappearance of the white contrast lines in the pore images.

Shrinkage curves of the radii of individual pores are reported in Fig. 7. Note that there are no data under 4 μm since this is the minimum radius that could be correctly determined by the pore detection software in combination with the present experimental setup. Two different parts can be observed in the shrinkage curves independently on the pore size. A first one, composed of few data points, with a large shrinkage rate, hereafter part I, and a second one with a smaller shrinkage rate, hereafter part II. Moreover some shrinkage curves are characterized by kinks appearing at the same annealing time. This corresponds to an increase of the pore sizes occurring between the end of the first annealing and the beginning of the second one. Actually the abscissa of peak of a kink correspond to the first measure at 800° of the second annealing, whereas that of the preceding data is related to the last measure at 800° of the first annealing cycle.

No changes on the shrinkage rates were revealed among pores of different size in the small range of pore sizes studied.

The global structural perfection of the sample after the annealing was studied by measuring the full width at half maximum (FWHM) of the rocking curve for the reflection $\tau^3(0/2\ 0/0\ 0/0)$. Using a beam size of $250\times250\ \mu m^2$, the FWHM before and after the annealing were 0.028° and 0.0031°, respectively, showing that the structural perfection has globally improved.

The chemical composition and the angular positions of Bragg reflections were checked, respectively, by SEM EDS analysis and high-resolution diffractometry in the sample after annealing. No changes were detected.

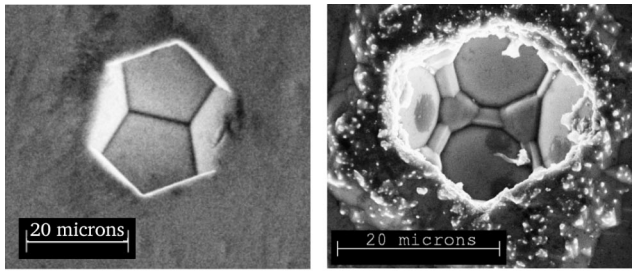

(a) before (b) after 2^{nd} cycle

FIG. 6. Scanning electron micrographs of a typical pore (a) before and (b) after the annealing. A further faceting at the edges of the annealed pore is clearly visible.

IV. DISCUSSION

The diffusion process in icosahedral Al-Pd-Mn has been studied as a function of the temperature by radiotracer techniques. Most of the diffusion experiments in icosahedral Al-Pd-Mn (Refs. 15–18) have shown that at temperatures above 450 °C the self-diffusion of ^{103}Pd, ^{54} Mn (no affordable radiotracer exists for aluminum) and the diffusion of foreign elements such as ^{65}Zn, ^{114}In, ^{195}Au is very similar to that of the same elements in crystalline Al, in which a vacancy-mediated diffusion mechanism is generally accepted. This opens the possibility to analyze the shrinkage curves (Fig. 7) in the frame of a diffusion annealing model developed by Volin and Balluffi.[19] They observed the isothermal shrinkage of nanometric pores in thin foils of pure aluminum by TEM. According to this model, atoms are transported to pores from sources at the external surfaces by the migration of vacancies. It is assumed that the local vacancy equilibrium is maintained at all the interfaces, and that the kinetics is therefore diffusion controlled. The local vacancy equilibrium depends on the curvature of the surface and therefore on the radius of the pores which are taken to be spherical in this model. Small pores have a high vacancy concentration in equilibrium at their surfaces. The model predicts an atomic flux proportional to the difference ΔC between the concentrations of vacancies at the pore surface and the sample surfaces. The radial shrinkage rate is given by

$$\frac{dr}{dt} = -\frac{D_s}{\xi r}\left[\exp\left(\frac{2\Omega\gamma}{rkT}\right) - 1\right], \tag{1}$$

where D_s is the self-diffusion coefficient, r is the pore radius, Ω is the atomic volume, γ is the surface energy, and ξ is a geometric factor usually taken equal to 1. The self-diffusion coefficient D_s, as determined from the data, was given by the following Arrhenius equation:

$$D_s = D_0 \exp\left(\frac{-Q}{kT}\right) = 1.76\times 10^{-5}\exp\left(\frac{-1.31\ \text{eV}}{kT}\right)\ \text{m}^2\ \text{s}^{-1}, \tag{2}$$

where D_0 is the preexponential factor and Q is the activation energy.

The current data were analyzed on the basis of this model using $\Omega = 14.92\times 10^{-30}$ m^3, according to the structural model of icosahedral Al-Pd-Mn quasicrystal developed by Boudard *et al.*,[3] and $\gamma = 0.886$ J/m^2 for the surface energy. This last value is the mean between the lower (0.6 J/m^2) and upper bounds (1.172 J/m^2) calculated by Fournee *et al.*[20] Using these values and considering the micrometric radii of pores, the argument of the exponential is small and the following approximation can be made:

$$\frac{2\Omega\gamma}{rkT} \ll 1,$$

$$\frac{dr}{dt} = -\frac{D_s}{r}\left[\exp\left(\frac{2\Omega\gamma}{rkT}\right) - 1\right] \simeq -\frac{D_s}{r}\left(\frac{2\Omega\gamma}{rkT}\right),$$

and after integration

$$r = \sqrt[3]{r_o^3 + \frac{6D_s\Omega\gamma}{kT}(t_0 - t)}, \tag{3}$$

where r_0 is the pore radius at the beginning of the annealing and t_0 is the initial annealing time. One can observe that the volume of the pore varies linearly with the time.

The pore shrinkage curves were fitted in order to calculate the diffusion coefficient D_s of both parts I and II. Part I was fitted linearly because of the small number of data, whereas part II was fitted according to Eq. (3). Figure 8 shows the shrinkage curve of two pores with its fitting curve. The second parts of the shrinkage curves are well described by the fitting curves. The diffusion coefficients calculated from each shrinkage curve for parts I and II are shown in Fig. 9 as a function of the initial pore radius, respectively. The diffusion coefficients of part I are mainly concentrated around a mean value of $D_{\text{I}} = 2.5\times 10^{-10}$ m^2 s^{-1}, whereas those of part II are spread out over a larger range with a mean value of $D_{\text{II}} = 2.6\times 10^{-13}$ m^2 s^{-1}. Although the error of the diffusion coefficient for part II fitted to a single shrinkage curve is small, each curve gives a different value. This produces a large dispersion of the coefficients that is related to the fact that

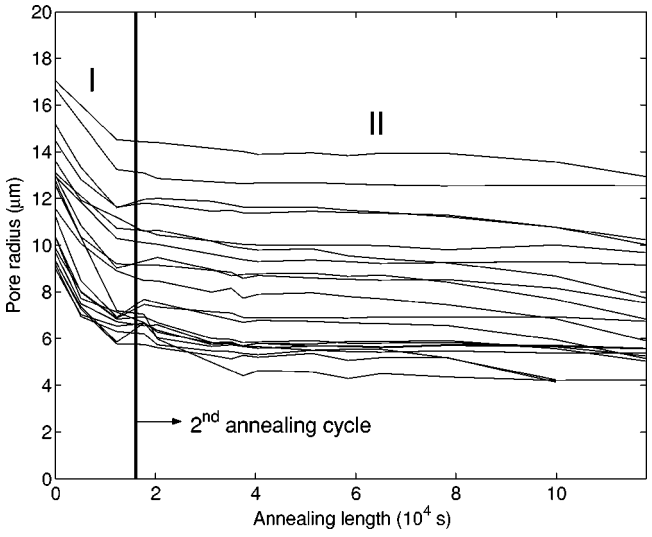

FIG. 7. Shrinkage curves of the radii of individual pores. The vertical line corresponds to the end of the first annealing cycle and the beginning of the second one.

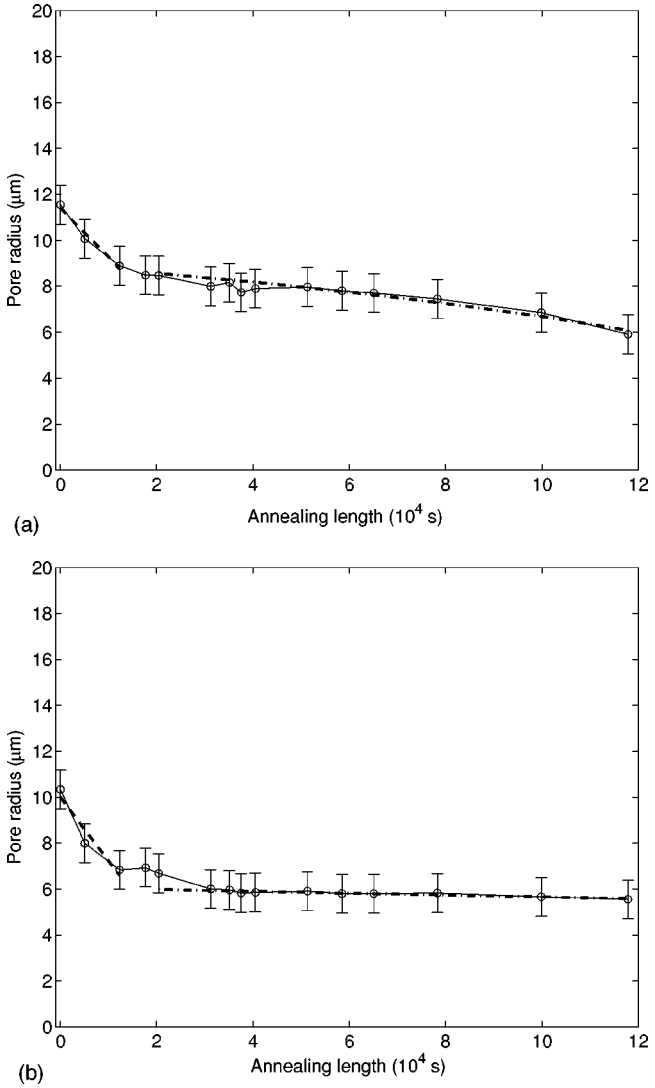

FIG. 8. Shrinkage curves of two individuals pores with the fitting curves in the parts I and II, respectively.

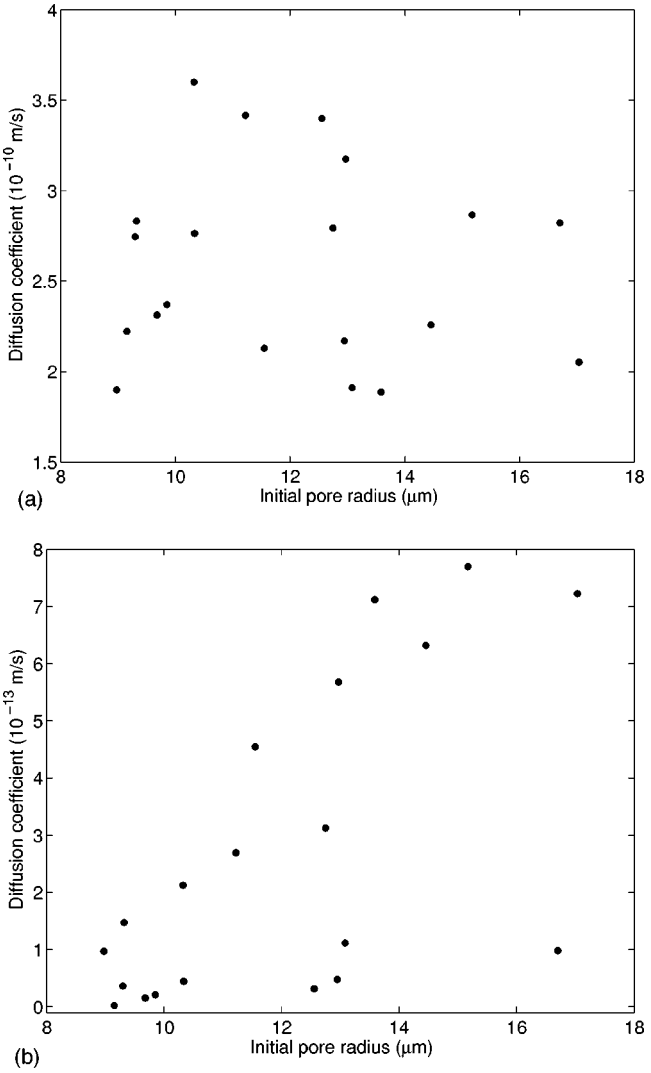

FIG. 9. Plot of the estimated diffusion coefficients of part I (a) and part II (b) as a function of the initial pore radius.

the part II varies from nearly flat to descendent (Fig. 8), i.e., pores do not shrink at the same time. The different shrinkage of part II might be due to a heterogeneous distribution of defects around pores, and to local variations of vacancies concentration because of an irregular oxidation of the external surfaces that does not allow them to act as perfect vacancies sinks. Nevertheless, the shrinkage follows the Volin-Baluffi model when pores start to shrink in part II. The self-diffusion coefficient for aluminum D_{Al}, estimated by Eq. (2), is equal to 1.3×10^{-13} m^2 s^{-1}. It was calculated for $T=612\,^{\circ}$C, which corresponds to the same homologous temperature T/T_{m} as the annealing temperature for *i*-Al-Pd-Mn ($T_{\mathrm{m}}=860\,^{\circ}$C). Comparing the diffusion coefficients D_{I} and D_{II} of the first and second shrinkage regime with that estimated for aluminum, the diffusion coefficient D_{I} is larger than that of aluminum, whereas the diffusion coefficient D_{II} is similar to that of aluminum. The second regime can therefore be attributed to a vacancy diffusion mechanism. The first regime, characterized by a higher shrinkage rate, could still be attributed to vacancy diffusion. Actually the presence of deformation in the sample in its as-grown state could have allowed vacancies to annihilate easily to the sample surfaces through the deformed lattice, leading to accelerated diffusion.[21,22] This hypothesis is consistent with the decrease of about an order of magnitude of the FWHM of the rocking curve which indicates a global lattice improvement.

A second possible origin of the fast shrinkage regime is an equilibration of the vacancy concentration in the bulk of the quasicrystal (QC). To illustrate this point let us consider the thermal history of the sample prior to our annealing experiment. The sample is first solidified at high temperature where it contains an equilibrium concentration of vacancies. In the course of the subsequent cooling the equilibrium concentration of vacancies drops as the temperature decreases. Part of the vacancies have enough time during this slow cooling to reach vacancy sinks (e.g., surfaces, grain boundaries, pores, etc.). In the present annealing experiment, the heating rate is higher than the cooling rate subsequent to solidification. When the sample reaches the annealing temperature of $800\,^{\circ}$C the vacancy concentration might therefore still be lower than the equilibrium value at this temperature. In this

case vacancies would be created at vacancy sources, which are the same as the sinks mentioned before, i.e., pores among others. Since the concentration gradient between the pore surface and the bulk of the QC would be much stronger than in the steady diffusion regime, so would be the shrinkage rate of the pores. Once the sample reached the equilibrium concentration of vacancies, a steady state diffusion regime can be established according to the model of Volin and Balluffi.

A hypothesis of the diffusion model is that pores are spheres with a constant radius of curvature. According to this hypothesis, the shrinkage rate of pores is predicted equal in each point of the spherical surface of pores. This does not correspond to the pores in Al-Pd-Mn quasicrystals that are dodecahedra, where the radius of curvature is not constant. In particular, at the flat facets the radius of curvature is nearly infinite, whereas at the edges or corners the radius of curvature would have to be considered very small. As a consequence, the shrinkage rate of pores takes different values at the facets, edges, and corners of the dodecahedron. The higher shrinkage rate at the edges and corners would mean that the pores are filled preferentially from the edges and corners, leading to the appearance of new facets as observed (Fig. 6). This leads thus to an increase of the radius of curvature at the edges and consequently to the smoothing of edges and the formation of new facets.

A change in the size and shape of some pore images was observed after the cooling of the sample at the end of the first annealing cycle [Figs. 5(c) and 5(d)]. This change was also observed in the shrinkage curves of some pores showing kinks at the time between the end of the first annealing and the beginning of the second one (Fig. 7). It can be also interpreted in the frame of Volin and Balluffi's model. Cooling the sample slowly to room temperature leads to a decrease of the equilibrium vacancy concentration, but cooling it rapidly, such as by quench, destroys this equilibrium. The surplus of vacancies in the bulk can, in the inverse process of the one described above, annihilate at the pore surfaces, increasing the pore size. Moreover the vacancy annihilation takes place preferentially at the edges of pores as expected from Volin and Balluffi's model, reducing the extension of the new facets that formed during the annealing at the edges of pores. This would lead to an increase of the sizes of pore images and to the appearance of white line contrasts, due to the newly formed edges, as observed after the end of the first annealing cycle. This effect was not observed after the cooling of the sample at the end of the second annealing cycle. This can be due to the fact that the pore was too small to distinguish small size variations. Moreover, the nearly round shape of the pores at this stage does not favor the reappearance of the edges.

The shrinkage of pores can be also considered as consistent with changes in the morphology of fivefold Al-Pd-Mn quasicrystalline surfaces observed after annealing at 600 °C by Schmithüsen *et al.*[23] The studied surfaces were mechanically polished and cleaned by ion sputtering in ultrahigh vacuum. Schmithüsen *et al.*[23] reported a roughening of the surface and the formation of micrometric sized pores along some scratches on the surface due to the mechanical polishing. A successive rearrangement of pores on the surface was observed according to the annealing length. Similar morphology changes on cleaved fivefold surfaces of icosahedral Al-Pd-Mn quasicrystals were also observed in the same temperature range by Ebert *et al.*,[24] Kluge *et al.*,[25] and Capello *et al.*[26] These surface morphology changes were explained as activated by bulk diffusion of vacancies toward the sample surfaces that produces a region depleted in vacancies adjacent to the sample and pore surfaces.

The shrinkage of pores in the bulk observed in this current work can confirm such a hypothesis of vacancy bulk diffusion, since one can suppose that part of the vacancies that annihilate at the sample surfaces originate from shrinking pores. Moreover, this also explains the observed surface changes from smooth to rough.

In contrast to what was reported in Refs. 8 and 27, we observed that all pores in the volume of the quasicrystal decreased in size during the annealing. Beeli *et al.*[8] interpreted the growth of the large pores at the expense of the smaller ones in terms of a classical Ostwald ripening. Such an interpretation can also be valid for our data, provided one take into account the small thickness of the sample ($\sim 380\ \mu$m) and one considers the surfaces of the sample as ''infinite'' pores. According to diffusion data,[18] the diffusion distance at 800 °C of the relatively slow diffuser ^{54}Mn in Al-Pd-Mn is more than 300 μm during 32 h annealing. This diffusion distance is even larger for the faster diffuser Al. The surfaces of the sample are therefore well in reach for any vacancy inside the sample.

According to the above-mentioned discussion, the observed shrinkage of pores can be explained by a vacancy-mediated diffusion mechanism. This result can be used to discuss the current hypotheses on the origin of porosity. Since the pores were not observed at their nucleation state, but later during a further annealing, the current results do not directly shed any light on the origin of pores. Nevertheless some comments on the origin of pores can be made from the observed evolution of their size and shape. According to the hypothesis on the condensation of thermal vacancies, these vacancies result from a supersaturation after the cooling of the ingot from higher temperatures.[8] The vacancy supersaturation resulting from a slow solidification, which is used to grow quasicrystals, seems very small with respect to that necessary to nucleate clusters of vacancies with a large volume fraction, such as that observed in Al-Pd-Mn quasicrystal (up to 0.7%).[28] This vacancy supersaturation can be estimated from that of aluminum, which is the principal component of the Al-Pd-Mn system. Moreover, the diffusion at high temperature in Al-Pd-Mn is vacancy mediated as in aluminum[15,16,18] with vacancy formation and migration enthalpies in Al-Pd-Mn similar to those in aluminum.[29] The vacancy supersaturation in aluminum is large only for large cooling rate (10^6 C/s),[30] and the volume fraction of pores in aluminum, formed by vacancy condensation, is smaller with respect to those in Al-Pd-Mn. Moreover, the pores are formed after the quench of the ingot and a successive annealing.[31,32] These porosity formation conditions in aluminum are thus different from the slow solidification conditions used to grow Al-Pd-Mn quasicrystals. Under these condi-

tions, only a very high concentration of thermal vacancies could allow to get large supersaturation values similar to the large porosity volume fractions in Al-Pd-Mn. To the authors' knowledge there is no estimation of the equilibrium concentration of thermal vacancies in Al-Pd-Mn and still less estimation of the vacancy supersaturation as a function of the grain cooling rate. However, vacancies concentration measurements showed a very high concentration of structural vacancies.[29] By their nature, these vacancies should not participate in the diffusion process provided that there are not structural changes. Nevertheless these changes could be generated at high temperature by the F2-F2M phase transition, even though the chemical composition of the studied sample does not fall into the range of compositions where these phase transitions are observed.[33]

According to the hypothesis of hierarchical porosity, pores are an intrinsic feature of the quasicrystalline structure and they should be in equilibrium with the surrounding matrix. Moreover the size distribution of pores should obey precise hierarchical rules. This is opposite to the drastic shrinkage of pores observed in this work and to the variation of the size distribution.[28] One could thus suggest that porosity is a type of defect resulting from the solidification process, such as from the instability of the solid-liquid interface. However a systematic study of the size and density of pores as a function of the different solidification processes and parameters has to be carried out in order to deeply elucidate this possibility.

V. CONCLUSIONS

The current work was dedicated to the evolution of porosity in the icosahedral Al-Pd-Mn quasicrystalline at high temperature. A shrinkage of pores was observed during the annealing and it was interpreted according to a vacancy diffusion model. Two shrinkage regimes were clearly identified. One regime is consistent with the predicted diffusion coefficient, whereas a faster one could be explained by an accelerated diffusion in the deformed structure or an equilibration of the vacancy concentration in the bulk. The purpose of the reported measure of the diffusion coefficients is only to provide an indication of the nature of the diffusion mechanism. Measures of the shrinkage of pores at different temperatures and for longer annealing lengths are being carried out in order to study the kinetics of pores and to get a deeper insight in their annealing behavior.

These results indicate an influence of the vacancy diffusion on the high-temperature evolution of porosity, which could support the hypothesis of vacancy condensation. Nevertheless both hypotheses on the porosity formation suppose that the distribution of pores would be uniform in the volume of quasicrystals. This is not consistent with the variation of the size distribution of pores in the volume of samples.[28] This variation could provide an indication of the influence of the solidification process on the porosity formation.[34] In order to check this hypothesis as well as to get an insight of the porosity nucleation mechanisms, *in situ* solidification experiments are currently in progress.

ACKNOWLEDGMENTS

The authors are very grateful to J. Bernardini for the fruitful discussions and to M. Boudard and M. de Boissieu from LTPCM for having provided high quality Al-Pd-Mn quasicrystalline samples. They would equally like to thank P. Cloetens for his help during the experiments. Finally the authors thank P. Retout and T. Bactivelane for the technical support before and during the experiments.

[1] D. Shechtman, I. Blech, D. Gratias, and J.W. Cahn, Phys. Rev. Lett. **53**, 1951 (1984).
[2] M. Cornier-Quiquandon, A. Quivy, S. Lefebvre, E. Elkaim, G. Heger, A. Katz, and D. Gratias, Phys. Rev. B **44**, 2071 (1991).
[3] M. Boudard, M. de Boissieu, C. Janot, G. Heger, C. Beeli, H.U. Nissen, H. Vincent, R. Ibberson, M. Audier, and J.M. Dubois, J. Phys.: Condens. Matter **4**, 10 149 (1992).
[4] J. Gastaldi, S. Agliozzo, L. Mancini, A. Letoublon, H. Klein, J. Härtwig, and J. Baruchel, Philos. Mag. **83**, 1 (2003).
[5] C. Janot, M. de Boissieu, S. Agliozzo, L. Loreto, R. Farinato, T.J. Sato, A.P. Tsai, and I. Grillo, Physica B **300**, 52 (2001).
[6] L. Mancini, E. Reinier, P. Cloetens, J. Gastaldi, J. Härtwig, M. Schlenker, and J. Baruchel, Philos. Mag. A **78**, 1175 (1998).
[7] S. Agliozzo and P. Cloetens (unpublished).
[8] C. Beeli, T. Godecke, and R. Luck, Philos. Mag. Lett. **78**, 339 (1998).
[9] C. Janot, L. Loreto, R. Farinato, L. Mancini, J. Gastaldi, and J. Baruchel, in *Quasicrystals*, edited by J.-M. Dubois, P.A. Thiel, A.-P. Tsai, and K. Urban, Mater. Res. Soc. Symp. Proc. No. **553** (Materials Research Society, Pittsburgh, 1999), p.55.
[10] C. Beeli and H.U. Nissen, Philos. Mag. B **68**, 487 (1993).
[11] P. Cloetens, R. Barrett, J. Baruchel, J.P. Guigay, and M. Schlenker, J. Phys. D **29**, 133 (1996).
[12] A. Snigirev, I. Snigireva, V. Kohn, S. Kuznetsov, and I. Schelokov, Rev. Sci. Instrum. **66**, 5486 (1995).
[13] J.C. Labiche, J. Segura-Puchades, D. van Brussel, and J. Moy, ESRF Newslett. **25**, 41 (1996).
[14] W. Kern, *Handbook of Semiconductor Wafer Cleaning Technology. Technology, Science and Application* (Williams Andrew Publishing, Noyes, 1993).
[15] R. Galler and M. Mehrer, in *Proceedings of the Seventh International Conference on Quasicrystals*, edited by F. Gahler, P. Kramer, H.R. Trebin, and K. Urban, Mater. Sci. Eng. A **294–296**, 693 (2000).
[16] R. Blüher, P. Scharwaechter, W. Frank, and H. Kronmüller, Phys. Rev. Lett. **80**, 1014 (1998).
[17] W. Spregel, T.A. Lograsso, and H. Nakajima, Phys. Rev. Lett. **77**, 5233 (1997).
[18] T. Zumkley, H. Mehrer, K. Freitag, M. Wollgarten, N. Tamura, and K. Urban, Phys. Rev. B **54**, R6815 (1996).
[19] T.E. Volin and R.W. Balluffi, Phys. Status Solidi **25**, 163 (1968).
[20] V. Fournee, A.R. Ross, T.A. Lograsso, J.W. Evans, and P.A. Thiel, Surf. Sci. **537**, 5 (2003).

[21] J. Philibert, *Diffusion and Mass Transport in Solids* (Les Editions de Physique, Paris, 1993).
[22] A.S. Ostrovsky and B.S. Bokstein, Appl. Surf. Sci. **175-176**, 312 (2001).
[23] F. Schmithüsen, Ph.D. thesis, Université J. Fourier, Grenoble, France, 2001.
[24] Ph. Ebert, F. Kluge, B. Grushko, and K. Urban, Phys. Rev. B **60**, 874 (1999).
[25] F. Kluge, Ph. Ebert, B. Grushko, and K. Urban, in *Proceedings of the Seventh International Conference on Quasicrystals*, Mater. Sci. Eng. A **294–296**, 294 (2000).
[26] G. Capello, I. Snigireva, V. Kohn, S. Kuznetsov, and I. Schelokov, Phys. Rev. B **65**, 245405 (2002).
[27] F. Kluge, M. Yurechko, K. Urban, and Ph. Ebert, Surf. Sci. **519**, 33 (2002).
[28] S. Agliozzo, E. Brunello, L. Mancini, H. Klein, J. Gastaldi, J. Härtwig, and J. Baruchel (unpublished).
[29] F. Baier, M.A. Müller, B. Grushko, and H.E. Schaefer, in *Proceedings of the Seventh International Conference on Quasicrystals*, Mater. Sci. Eng. A **294–296**, 650 (2000).
[30] C. G'sell, Ph.D. thesis, Université de Nancy I, Nancy, France, 1971.
[31] K. Ono and T. Kino, Philos. Mag. A **81**, 2565 (2001).
[32] M. Kiritani, Y. Shimomura, and S. Yoshida, J. Phys. Soc. Jpn. **19**, 1624 (1964).
[33] I. Hirai, T. Hishimasa, A. Letoublon, M. Boudard, and M. de Boissieu, in *Proceedings of the Seventh International Conference on Quasicrystals*, Mater. Sci. Eng. A **294–296**, 33 (2000).
[34] A.R. Ross, I.R. Fisher, P.C. Canfield, and T.A. Lograsso, in *Quasicrystal—Preparation, Properties and Applications*, edited by E. Berlin-Ferré, P.A. Thiel, A.-P. Tsai, and K. Urban, Mater. Res. Soc. Symp. Proc. No. **643** (Materials Research Society, Pittsburgh, 2001), p. K.1.5.1.